Power Density Improvement in Integrated Electromagnetic Passive Modules With Embedded Heat Extractors

Wenduo Liu, Jaco Dirker, and Jacobus Daniel van Wyk, *Fellow, IEEE*

***Abstract*—In this paper, heat extractors are embedded into the magnetic materials of the integrated power electronics passive modules. The optimum volume of heat-extracting material may slightly reduce the amount of electromagnetic energy that is processed, but more efficient heat removal yields higher allowable levels of both electromagnetic stress and losses per unit volume in the remaining material. Without influencing the electromagnetic performance, heat extractors provide the potential to improve the power density of passive modules. This paper introduces the mechanism of heat extractors into passive power electronics modules. Theoretical thermal models and simulation are used to investigate factors influencing the module performance and the improvement on power density. Prototypes are built for experimental investigation. The experimental results show great improvement of power density by the application of heat extraction technology. High power density, more than 1 kW/in^3 (70 W/cm^3), is achieved on the prototype.**

***Index Terms*—Embedded heat extractor, passive integrated power electronics module, power density.**

I. Introduction

FOR A LONG time, pursuing high power density has been the trend in power electronics applications. With the application of high-density integration technology and the corresponding optimization designs for integrated power electronics modules, high power density of up to 480 W/in^3 (29 W/cm^3) has been achieved in passive modules with the operating frequency of 1 MHz [1]. Associated with the increase of power density, the increasing loss density leads to thermal issues in practical applications. The maximum allowed temperature inside modules has become the main design limitation for passive power electronics modules. While the surface temperature of a module can be controlled by external cooling conditions, the maximum temperature rise inside the module is determined by its heat-conduction ability, which describes the capability of a module to disperse inner heat to the outside. The heat-conduction ability of a passive module is influenced by the distribution of generated heat, the structure, and the material properties, including the thermal-interface performance. For a specific module with fixed heat distribution, the maximum temperature difference between the inside and the surface of the module has been proposed to represent the heat-conduction ability [2].

A large part of the volume of a passive power electronics module includes ceramics with low average thermal conductivity [3]. To improve its heat-conduction ability, the concept of embedded heat extractors has been proposed, and is proven to be a feasible approach [4]. The embedding of electromagnetically inactive heat-extracting material reduces the effective volume of the electromagnetic material, thus increasing the loss density; on the other hand, it provides additional heat-extraction channels and changes the distribution of the generated heat by separating heat-generating material with non-heat-generating materials. An improvement in the efficiency of heat removal yields higher allowable levels of both electromagnetic stress and loss density in the remaining electromagnetic materials, providing the potential to increase the power density. In practical design procedures, a tradeoff exists between high efficiency and high power density; this can be controlled by different criteria.

Based on the study of a specific integrated passive module, this paper investigates the application of ceramic heat extractors in passive power electronics modules. To improve the heat-conduction ability, the ceramic heat extractors are inserted into a module. The construction and material characteristics of the improved module are discussed in Section II. The electromagnetic design of an integrated logical link control translator (LLCT) module and its loss distribution is presented in Section III. In Section IV, the factors influencing the thermal behavior of the improved module are discussed. Numerical simulation results and the discussions are presented in Section V. The verification experiments are presented in Section VI.

II. Passive Module With Embedded Heat Extractors

An integrated passive module combines capacitive and inductive (as well as transformative) functions in a module [5] (refer to Fig. 3). Providing sufficient inductance generally requires a magnetic material such as a ferrite core. The dimensions of the

Manuscript received September 14, 2006; revised October 3, 2007. First published October 28, 2008; current version published December 9, 2008. This work was supported in part by the Engineering Research Centers (ERC) Program of the National Science Foundation under Award EEC-9731677. Recommended for publication by Associate Editor B. Ferreira.

W. Liu was with the Center for Power Electronics Systems at Polytechnic Institute and State University of Virginia, Blacksburg, VA 24060 USA. He is now with the International Rectifier Corporation, El Segundo, CA 90245 USA (e-mail: wliu1@irf.com).

J. Dirker was with the Center for Power Electronics Systems at Polytechnic Institute and State University of Virginia, Blacksburg, VA 24060 USA. He is now with the Department of Mechanical and Aeronautical Engineering, University of Pretoria, Pretoria 0002, South Africa (e-mail: jaco.dirker@up.ac.za).

J. D. van Wyk was with the Center for Power Electronics Systems at Polytechnic Institute and State University of Virginia, Blacksburg, VA 24060 USA. He is now with the Department of Electrical and Electronic Engineering Science, University of Johannesburg, Auckland Park Campus, Johannesburg, South Africa (e-mail: daanvw@uj.ac.za).

Color versions of one or more of the figures in this paper are available online at http://ieeexplore.ieee.org.

Digital Object Identifier 10.1109/TPEL.2008.2005367

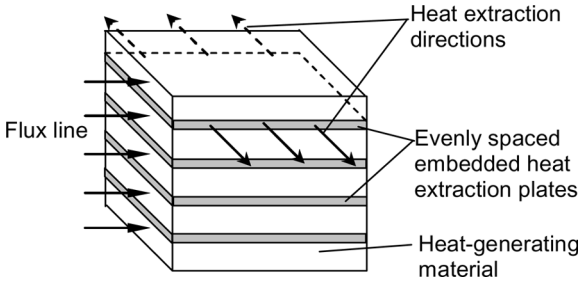

Fig. 1. Optimum heat extraction geometry for cases in which heat-extractor material occupies less than 10% of the total volume.

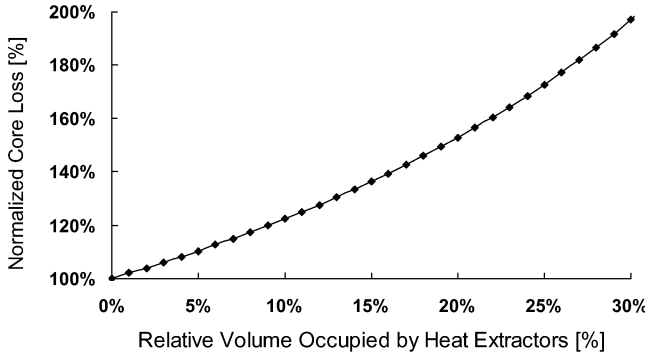

Fig. 2. Normalized power loss vs. relative volume of heat extractors.

core are determined not only by the electromagnetic specifications but also by the allowed core loss density. In cases where efficiency is not the main design consideration, the maximum allowed core loss density is set to limit the maximum temperature inside the module to be lower than a practically acceptable value, for example, 100 °C. It is obvious that by improving the thermal-removal ability of the module, the core can support a higher loss density, which normally corresponds to a higher power density.

A solid-state heat extractor has been proposed to improve the heat-conduction ability of cores in passive modules [4]. Heat extractors are embedded into cores to provide additional heat-transfer paths, as shown in Fig. 1. In practical applications, the embedding of heat extractors is not supposed to change the overall dimensions of the original module. Toward this end, a certain amount of the core is replaced by the heat extractors. Since the flux is kept constant, reducing the core volume increases the flux density and core loss density, and thus, changes the core loss. Assuming the module is excited with sinusoidal waveforms, the Steinmetz equation, (1), can be applied to estimate the core loss. The core loss density is calculated by the frequency, flux density, and material constants

$$P_v = C_1 f^{C_2} B^{C_3}. \tag{1}$$

The normalized core loss with respect to the relative volume occupied by heat extractors is described in (2), where C_3 is the parameter in the Steinmetz equation that represents the material constant, which has a typical value of 2.9 for 3F4 material at 1 MHz (manufacturer data); and α is the relative volume of heat extractors, which is the ratio of the volume of heat extractors to the total volume

$$P_n = \frac{P_{\text{loss}}(\alpha)}{P_{\text{loss}|\alpha=0}} = (1-\alpha)^{1-C_3}. \tag{2}$$

Fig. 2 shows that by replacing 10% of the core with heat extractors, the core loss will increase to 122% of the original amount. To maintain high efficiency, normally the reduction of core volume is expected to be less than 10%. The numerical optimization investigation shows that the optimal cross-sectional shape of solid-state embedded heat extractors is that of continuous flat layers, as shown in Fig. 1 [6]. An added attraction for this approach is that heat extractors with flat structures offer easy assembly.

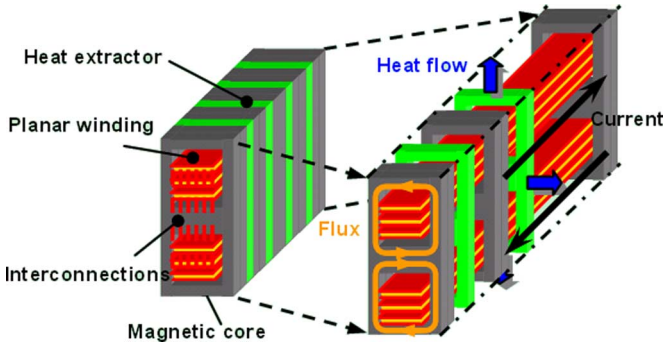

Fig. 3. Method of inserting heat extractors into an integrated module.

The location of heat extractors is another consideration for assembly. To avoid influencing the magnetic characters of the module, the heat extractors should be located parallel to the flux lines, so that flux lines have minimal crossing of the interfaces between the ferrite and the heat extractors. Thus, the heat extractors have the same cross-sectional shape as the core, and are inserted evenly into the ferrite cores, as shown in Fig. 3. For this kind of structure, heat sinks are placed on the four side surfaces of the module in order to perform three-dimensional heat extraction.

To avoid generating additional heat, the heat-extractor material should be electromagnetically inactive. Aluminum nitride is selected as the solid-state heat-extraction material for high cost-efficiency and thermal conductivity, of which the achieved level is 170 W/m·K; this is much higher than that of ferrite, which is about 5 W/m·K.

Besides thermal conductivities, the interfacial thermal resistance also influences the overall thermal performance. As reported in other research [4], when there is an increase in either the thermal contact resistance between the core and heat extractors or the thermal contact resistance between the module and the heat sink, there is a resulting increase of the barriers in the thermal path; thus, the benefit of heat extraction is reduced. Thermal adhesives, such as silver loaded paste, are used to mechanically bind ferrite cores and heat extractors, and to reduce the interfacial thermal resistance to 2×10^{-4} (m^2·K)/W (manufacturer's data). Noting that the interfacial thermal resistance is influenced by the contact pressure, mechanical clamps are

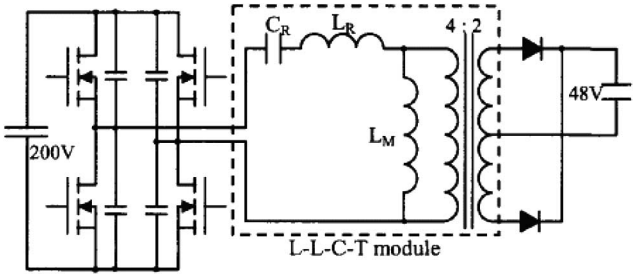

Fig. 4. Converter circuit showing components replaced by LLCT module.

applied to fix the module and the heat sinks, and to reach the interfacial thermal resistance of 2.3×10^{-4} ($m^2 \cdot K$)/W, measured in [2].

In the previously mentioned work [4], the core is the only heat generator; thus, heat extractors are supposed to remove only the heat inside the cores. Heat transfers one way from the core to the extractors. For this kind of application, the interfacial thermal resistance is the dominant barrier in the heat path, and thus, plays an important role in influencing the overall thermal performance of the module. However, in a practical passive power electronics module, the integrated conductor and dielectric materials create an amount of heat comparable to that generated by the core. For example, the sum of conductor loss and dielectric loss in previously designed integrated LLCT modules occupies about 80% of the total module loss [7]. In such a module, considerable heat is generated in the kernel of the module. On its way to the heat sink, the heat may induce a large temperature rise due to the internal thermal resistance, such as the thermal contact resistance between the winding materials and the magnetic core, the thermal resistance of the core, and the thermal contact resistance between the core and the heat sink. Here, heat extractors provide not only a channel for extracting heat generated inside the core, but also a path to transfer the heat inside the kernel to the heat sink. The overall thermal performance of a module with heat extractors is not only determined by the material properties, but also the structure of the module and the distribution of the loss.

III. Integrated LLCT Module

A specific passive module is presented as the example, in which the factors influencing the module performance can be investigated. The integrated LLCT module, as the name indicates, has the equivalent function of the combination of four discrete components: magnetizing inductor, resonant inductor, resonant capacitor, and transformer, as shown in Fig. 4. This module is designed for a 500 W dc/dc series resonant converter, converting 200 V input to 48 V output, with an operating frequency of 1 MHz. The design specifications are listed in Table I. The operation of the LLC resonant circuit is discussed in other work [8].

The stacked structure is applied to implement the module [9]. The integrated module is built based on a transformer with planar windings. In the primary side, eight inductor–capacitor (L–C) cells are connected as a four-turn winding. The L–C cells are made by long, thin dielectric strips covered by copper layers on both sides. The dielectric material is ceramic NPO1250 with a relative permittivity of 186 and a thickness of 0.15 mm. The copper layer has a thickness of half copper skin depth at 1 MHz. By properly setting the terminals and interconnections, the L–C cell winding functions as an inductor–capacitor series resonator. The secondary winding is made of thin copper foil. Between the two windings, a thin ferrite polymer composite (FPC) strip is used to provide leakage inductance. Both the windings and the leakage layer are encapsulated with epoxy. Two planar ferrite cores surround the encapsulated block with an adjustable air gap. The structure diagram is shown in Fig. 5.

The dimensions of the module are determined by the values of the two design variables, the magnetic flux density B, and the average current density J. Proper design can be achieved based on different criteria of efficiency and power density. The optimal design shows the potential of this structure to reach high power density, but before the design is finally determined, the maximum allowed temperature rise should be considered as a constraint. To sufficiently narrow the research focus of this study, the authors have avoided selecting designs with high loss density, which may not allow for practical implementation in the verifying experiments. The selected design is the one with an average current density of 10 A/mm^2, a flux density of 55 mT, and an estimated power loss of 17 W. The dimensions of the module are listed in Table II, and the loss distribution is listed in Table III.

TABLE I
Design Specifications

Parameters	Values
resonant inductance, L_r	0.4 mH
resonant capacitance, C_r	50 nF
resonant frequency, f_r	1.1MHz
magnetizing inductance, L_M	20 mH
operating frequency, f	1 MHz
turn's number in primary, n_p	4
turn's number in secondary, n_s	2
connection method of L-C cells	Parallel
current in primary, I_{prirms}	3.09A
current in secondary, I_{secrms}	10.5 A
output power, P_{out}	500W

TABLE II
Dimensions of the Integrated Module

Dimension Parameters	Values
winding window width	11 mm
winding window height	3 mm
core thickness	2 mm
module width	15 mm
module height	14 mm
module length	60 mm

TABLE III
POWER AND LOSSES APPLIED IN THE THERMAL MODEL

Parameters	Values
winding loss	5 W
dielectric loss	1W
core loss	11.3 W

IV. FACTORS INFLUENCING THE THERMAL PERFORMANCE

To investigate how heat extractors influence the performance of the module, a simplified thermal model is built based on the structure shown in Fig. 5. Since it is not the intention of this paper to present a detailed thermal analysis, the simplified model is used here to give a qualitative discussion of the main considerations.

Several assumptions are made to simplify the model. In the windings, thin dielectric layers and thin copper layers interleave and stack tightly within an encapsulant package. The winding and the encapsulant together are regarded as a uniform heat-generating block with the same thermal conductivity as the dielectric material, 0.2 W/m·K. Since heat extractors do not contact the inner part of the winding block, this approximation changes the internal temperature rise of the winding block, but has only slight influence on the module performance as it relates to heat extractors.

The ferrite core is regarded as a uniform heat-generating medium. The thermal contact resistance between the core and the winding block is assumed to have the same value as that between the heat extractors and the winding block, and is termed as the internal thermal contact resistance, $R_{\rm in}$. The thermal contact resistance between the core and the heat sink is assumed to have the same value as that between the heat extractors and the heat sink, and is termed as the external thermal contact resistance, $R_{\rm ext}$.

As shown by the dimensions given in Fig. 5, the module length is much larger than the width and height. Thus, a two-dimensional heat transfer can be assumed on the cross section. Fig. 6 shows the diagram of heat paths on the cross section. In a module, there are two heat sources: the winding block and the magnetic core. Applying the superposition principle, the amounts of heat flux generated by these two heat sources can be studied separately, and the results can be combined linearly. For the heat generated inside the winding block, both the core and heat extractors are conduction paths, through which heat can be conducted to the heat sink. The internal and external thermal contact resistance and the equivalent thermal resistance of the combination of the core and heat extractors are the barriers on this heat path. For heat generated in the core, the winding block functions as a conductor conducting heat between the core and the heat extractors. Because of the different heat distribution, the equivalent thermal resistance with respect to the two heat sources is different. The equivalent structures of both cases are shown in Fig. 6, where the core and the winding block are replaced by equivalent spot heat sources, and the corresponding equivalent thermal resistance is applied.

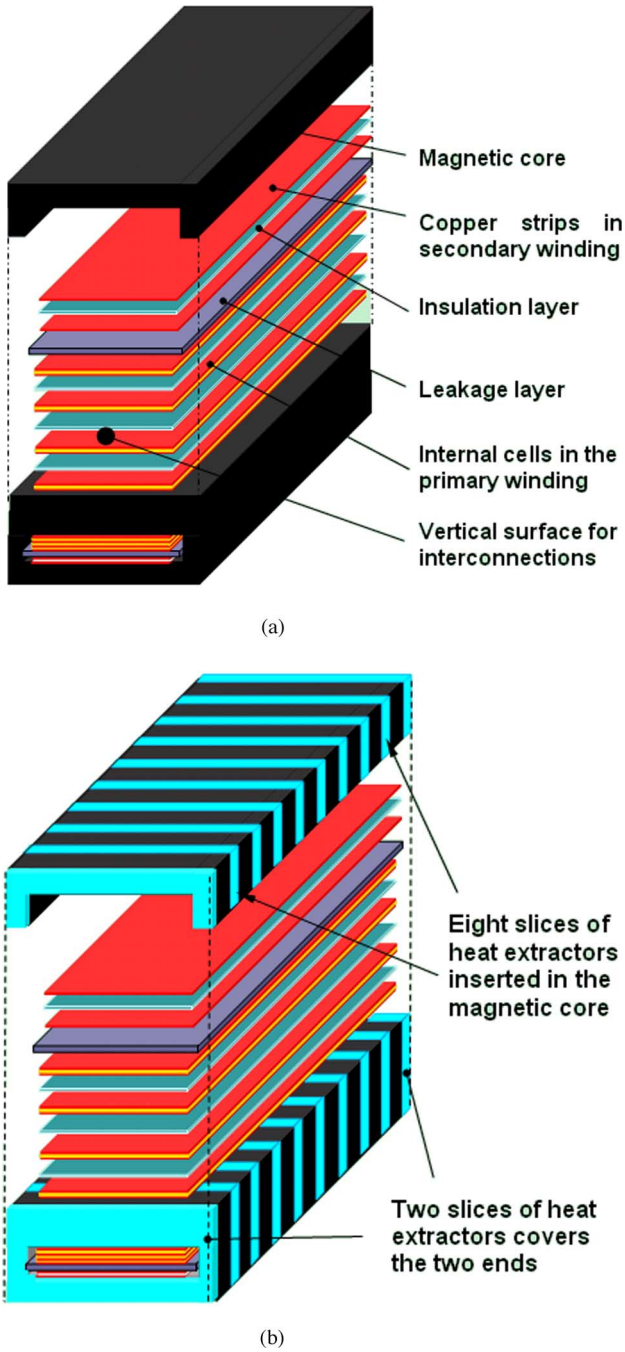

Fig. 5. (a) Exploded view of the LLCT module without heat extractors. (b) Exploded view of the LLCT module with heat extractors.

The relative volume of heat extractors influences both the core loss and the thermal resistance on the heat paths, while the interfacial thermal resistance between the core and heat extractors, R_{Fe-AlN}, does not have much impact on the thermal performance. The interfacial thermal resistance becomes less important in cases where the core thickness is much smaller than the width and height of the module, because a small core thickness leads to a small area of contact with the heat extractors. Heat transfers directly to the heat sink without passing the heat extractors. The amount of heat conveyed between the core and

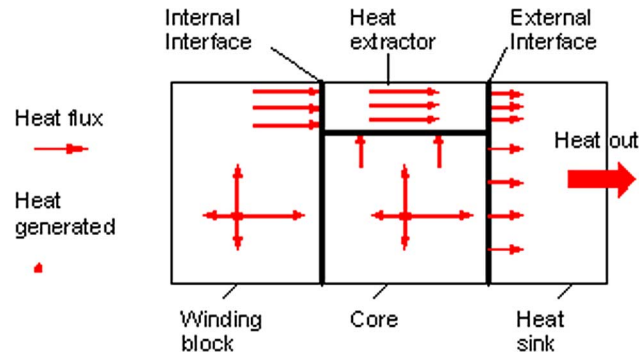

Fig. 6. Diagram of heat paths on cross section.

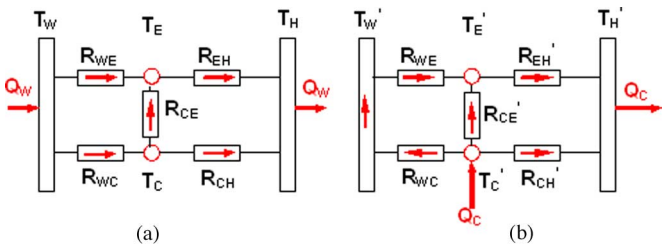

Fig. 7. Equivalent structure (a) for removing heat in the winding block and (b) for extracting heat from the core.

heat extractors is also related to the heat-generation distribution and detailed boundary conditions.

In some applications, the loss in the winding block will be much higher than that in the core. If the core thickness is much smaller than the cooling area contacting the heat sink—for example, a planar core is applied—the thermal resistance between the core and heat extractors, R_{CE}, is so large that the heat conduction between the core and heat extractors is negligible. For such cases, it can be assumed that no heat transfer occurs between the core and the heat extractors, and the model in Fig. 7(a) can be solely applied. Assuming that the value of R_{CE} is infinite, the overall equivalent thermal resistance of the module can be expressed by the following:

$$R_o = \frac{(k_n R_s + R_{\rm core})(R_s + R_{\rm core})}{(k_n R_s + R_{\rm core}) + (k_n - 1)R_{\rm core} \cdot \alpha} \qquad (3)$$

where k_n is the ratio of the heat-extractor thermal conductivity to the core thermal conductivity, R_s is the sum of the internal and external interface thermal resistances, $R_{\rm core}$ is the thermal resistance of the core without embedded heat extractors, and α is the relative volume of heat extractors. The value of overall equivalent thermal resistance R_o varies within the range as $R_s + (R_{\rm core}/k_n) \le R_o \le R_s + R_{\rm core}$. If thermal adhesive with high thermal conductivity is applied in the internal and external interface, the value of R_s can be small; then, the overall equivalent thermal resistance is approximately inversely proportionate to the relative volume of the heat extractors.

In some applications, the core loss is the dominant loss of the module, and the core thickness is comparable to the width and height of the module. Then, the model in the Fig. 7(b) can be solely applied. Ignoring the heat passing through the winding block, the investigations for this model are carried out with

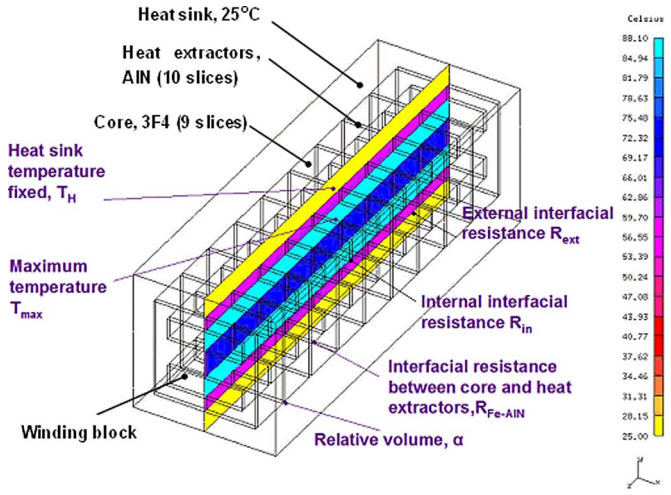

Fig. 8. Finite-element method (FEM) model of the integrated LLCT module with embedded heat extractors.

numerical methods, and these results are verified by experiments in other work [4].

However, in those power electronics applications where the optimal design is to reach highest power density, the core loss is comparable to the winding loss and the dielectric loss, and core thickness is not negligible. For heat generated by the winding loss and the dielectric loss, the heat extractors directly perform as heat dissipation paths. Thus, in these cases, the relative volume of heat extractors has more influence on the reduction of temperature rise than those presented in [2] and [4]. For these cases, such as the integrated LLCT module presented in Section III, numerical methods must be applied in the investigation.

V. Thermal Simulation and Discussions

Based on the assumptions discussed in Section IV, a thermal model was built in the simulation software, I-DEAS, to investigate the factors influencing the performance of the module with heat extractors, as shown in Fig. 8.

The model consists of nine core layers and ten aluminum nitride layers. The two kinds of layers interleave with each other. By changing the thickness of the layers, the relative volume of heat extractors can be controlled. The thermal resistance on the interfaces is determined by materials and processing technologies. The internal thermal contact resistance is estimated by calculating the thermal resistance between the winding block and the inner surface of the core and heat extractors. The material in between can be either air[(1)] or the encapsulant[(2)] with a thermal conductivity of 1.5 K/m·W. The material between the heat sink and the outer surface of the module can be either thermal adhesive[(3)] or a thermal pad[(4)]. The interfacial thermal resistance between the core and heat extractors is obtained from the measurement results in [2]. By changing the surface roughness and the applied pressure, the interfacial thermal resistance can be modified. The values of the thermal contact resistance and the corresponding interfacial thermal resistance are listed in Table IV. In the simulation, the temperature on the heat sink

TABLE IV
PARAMETERS VALUES IN THE SIMULATION

	Thermal Contact Resistance [K/W]	Interfacial Thermal Resistance [m^2K/W]
$R_{in}^{(1)}$	7.44	2.5 x 10^{-2}
$R_{in}^{(2)}$	0.198	3.3 x 10^{-4}
$R_{ext}^{(3)}$	0.072	2.5 x 10^{-4}
$R_{ext}^{(4)}$	0.718	2.5 x 10^{-3}
$R_{Fe\text{-}AlN}$	1.39	2 x 10^{-4}

The notation (1), (2), (3), (4) are corresponding to materials discussed before.

TABLE V
PARAMETERS FOR THE SIMULATION OF GROUP 1 AND GROUP 2

	Group 1	Group 2
ΔT_{max} for $\alpha = 0$ [°C]	15.4	63.1
R_{in} [m^2K/W]	3.3 x 10^{-4}	2.5 x 10^{-2}
R_{ext} [m^2K/W]	2.5 x 10^{-4}	2.5 x 10^{-3}
$R_{Fe\text{-}AlN}$ [m^2K/W]	2 x 10^{-4}	2 x 10^{-4}

surface is fixed at 25 °C. The two terminal surfaces are set as thermal isolation.

Since the varying relative volume of the heat extractor changes the loss as well as the loss distribution in the core, the module with the best thermal-handling ability may not be the one with the minimum temperature rise. Thus, the overall equivalent thermal resistance cannot be representative of the performance of a module. The maximum temperature difference between the inside of the module and the heat sink surface, $\Delta T_{\max}$, is accommodated to represent the performance of the module. The lower internal temperature rise refers to better performance and also the larger power-processing capability.

Four factors influencing the performance of modules with heat extractors—the internal and external thermal contact resistances, the interfacial thermal resistance between the core and the heat extractors, and the relative volume of the heat extractors—were set as four respective variables in four different groups of simulation experiments.

For each group, the internal temperature rise in the module without a heat extractor was first obtained by simulation. This result was compared with the other results in the group. The module performance was then presented with normalized values of the internal temperature rise.

A. Investigation of the Influence of the Relative Volume of Heat Extractors, α

The simulation to investigate influence of the relative volume of heat extractors is made in two groups with different interface materials. In group 1, the air and thermal pad are the interface materials, while in group 2, the encapsulant and thermal adhesive are the interface materials. The temperature rise inside the module is obtained from simulation with the two groups of interface materials, respectively. The results and the values of corresponding contact thermal resistance are listed in Table V. Fig. 9 shows that by applying a small volume of heat extractors, the internal temperature rise decreases. The optimal value of the

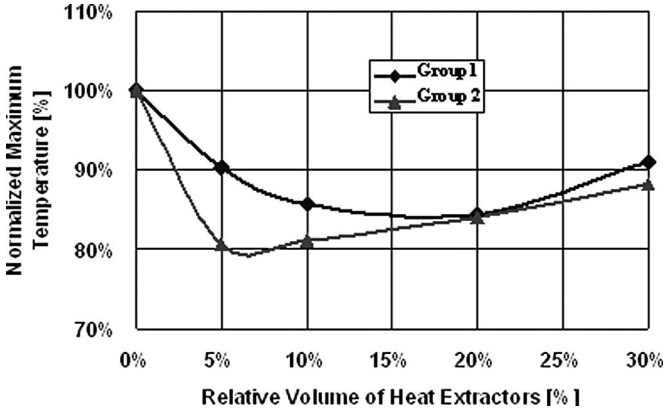

Fig. 9. Normalized maximum temperature difference vs. relative volume of heat extractors.

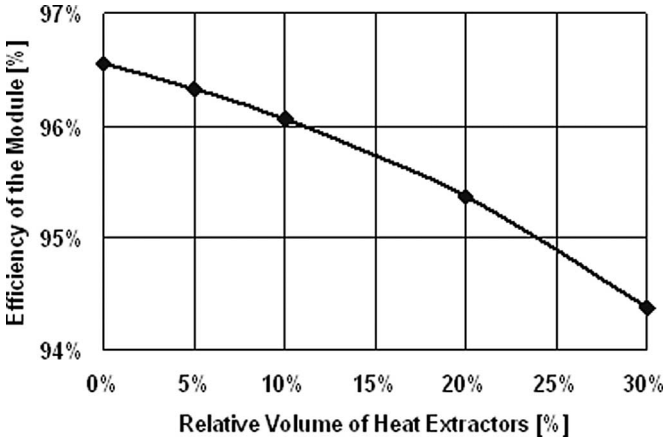

Fig. 10. Efficiency vs. relative volume of heat extractors.

relative volume of heat extractors varies with different interface thermal properties. In the practical design, before the optimal design of the relative volume, the interfacial material needs to be properly selected to determine the values of the interface thermal properties. For the presented module, with the heat extractors occupying 15% of the total volume, the internal temperature rise could be reduced to 85% of the original value with the efficiency reduction of about 1%, as shown in Fig. 10. In other words, with the application of heat extractors, the throughput power and the power density of the module can increase to 118% while the maximum temperature remains unchanged, assuming that the increased power loss is proportionately distributed into the winding block and the core.

B. Investigation of the Influence of the Interfacial Thermal Resistance Between Core and Heat Extractors, $R_{\mathrm{Fe-AlN}}$

To eliminate the influence from the internal and external contact thermal resistances, the values of the contact thermal resistance are fixed as 2×10^{-4} (m^2·K)/W in the simulation. The relative volume of heat extractors is set as 10%. The internal temperature rise in the module without a heat extractor is set as the comparison reference. Fig. 11 shows that the interfacial thermal resistance between the core and heat extractors has a slight influence on the thermal performance of this module.

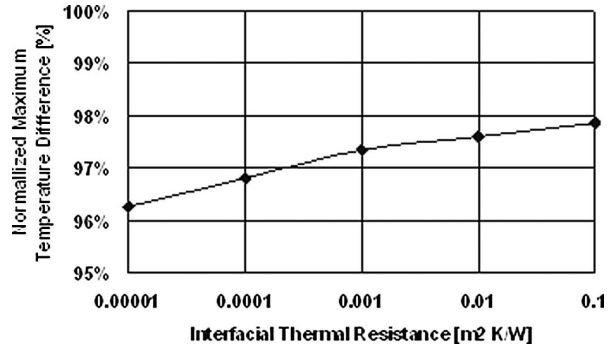

Fig. 11. Normalized maximum temperature difference vs. the thermal resistance between the core and heat extractors.

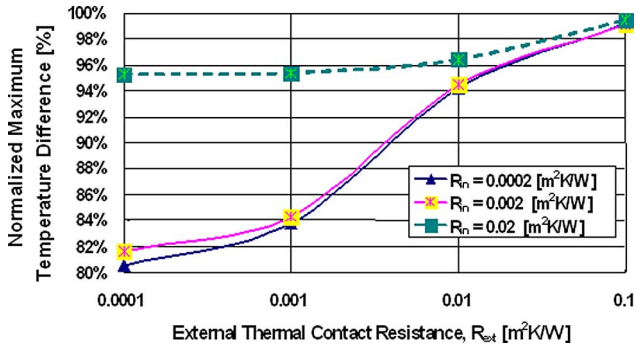

Fig. 12. Normalized maximum temperature difference vs. internal and external contact thermal resistances.

C. Investigation of the Influence of the Internal and External Contact Thermal Resistance, $R_{\rm in}$ and $R_{\rm ext}$

The relative volume of heat extractors for this simulation is set at 10%, and the interfacial thermal resistance between the core and heat extractors is set as 2×10^{-4} ($m^2 \cdot K$)/W. With the varying values of $R_{\rm in}$ and $R_{\rm ext}$, the internal temperature rise is obtained for modules with and without heat extractors, respectively. The two sets of values are compared to demonstrate the extent to which the internal temperature rise could be reduced by applying the heat extractors. Fig. 12 shows that the smaller the contact thermal resistance, the greater the improvement contributed by heat extractors is. As observed from the curves, when the internal thermal contact resistance $R_{\rm in}$ is large, say, at the level of 0.02 ($m^2 \cdot K$)/W, it exerts the main influence on the temperature reduction; when the $R_{\rm in}$ value reduces to the lower level as 0.002 ($m^2 \cdot K$)/W, it has less influence than the external thermal contact resistance, $R_{\rm ext}$. The reason is that when the $R_{\rm in}$ value is low enough, it impacts the internal paths of heat flow little. So does the $R_{\rm ext}$. The detailed threshold values depend on the specific structure, material properties, and the loss distribution.

VI. Verification Experiments

To verify the improvement made by heat extraction technology, two prototypes have been built to experimentally investigate the influence of applying heat extractors in passive integrated modules. Prototype I has the same structure and dimensions as the one without the heat extractor in the simulation. Prototype II has the same winding structure, dimensions, and materials as prototype I, but has 10% of the ferrite core replaced by heat extractors. The external views of the two prototypes are shown in Fig. 13. The heat extractors are made of aluminum nitride and have the same dimensions as indicated in the simulation structure. The two prototypes are tested with a 1 MHz inductor–inductor–capacitor (*LLC*) converter. The experimental and measurement setups are shown in Fig. 14. The LLCT total loss is measured by monitoring the heat dissipation at thermal steady state using a specific structure. A specific structure has been developed to monitor the heat flux flowing out for the LLCT module. Mechanical constraint was applied to eliminate the system measurement error. The relative uncertainty of the measured power loss is 4%. The details of this measurement are presented in [10]. The efficiency of the LLCT module and the whole converter, as well as the temperature at the thermal steady state, were recorded and compared. Since the loss distribution in the in-circuit test is different from the situation used in the thermal simulation, the experimental results are not comparable with the simulation results. Nevertheless, the experimental results between the two prototypes can be

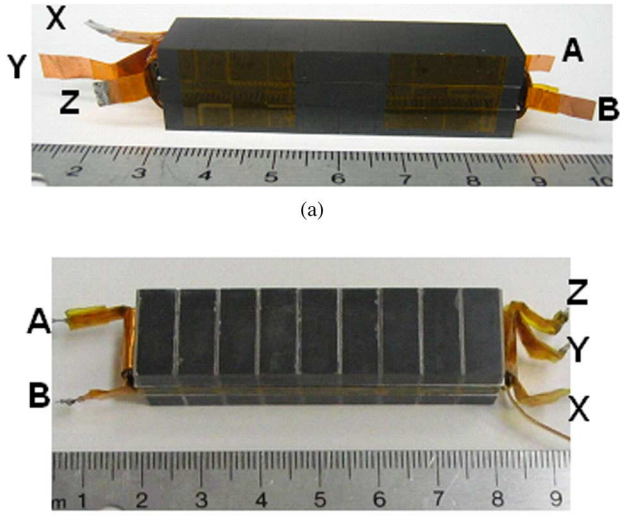

Fig. 13. Integrated LLCT modules with the identical winding structure and overall dimensions. (a) Prototype I: the integrated LLCT module without heat extractors. (b) Prototype II: the integrated LLCT module with heat extractors—ten pieces of AlN slices and nine pieces of ferrite cores.

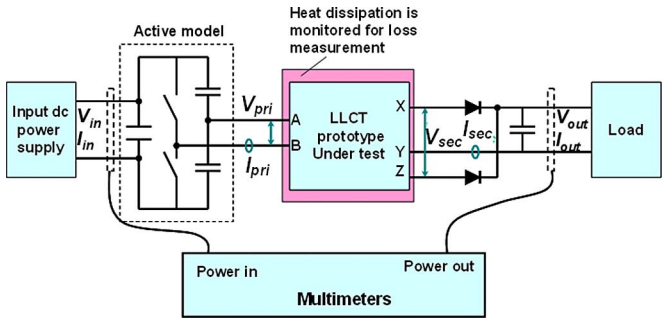

Fig. 14. Block diagram showing the experimental setup and measurement.

TABLE VI
CIRCUIT OPERATION CONDITIONS OF THE COMPARISON EXPERIMENTS

	Experiment	1	2	3	4	5
f (kHz)	prototype I	960	960	950	990	997
	prototype II	952	952	951	951	951
V_{in} (A)	prototype I	302.0	326.4	353.7	285.0	302.7
	prototype II	302.9	328.5	351.4	277.4	294.0
I_{in} (A)	prototype I	1.356	1.458	1.594	2.331	2.469
	prototype II	1.400	1.534	1.640	2.420	2.568
V_{out}(V)	prototype I	44.08	47.64	51.99	39.45	41.91
	prototype II	44.89	48.74	52.22	39.54	41.99
I_{out}(A)	prototype I	8.70	9.37	10.20	15.63	16.57
	prototype II	8.84	9.70	10.37	15.63	16.58

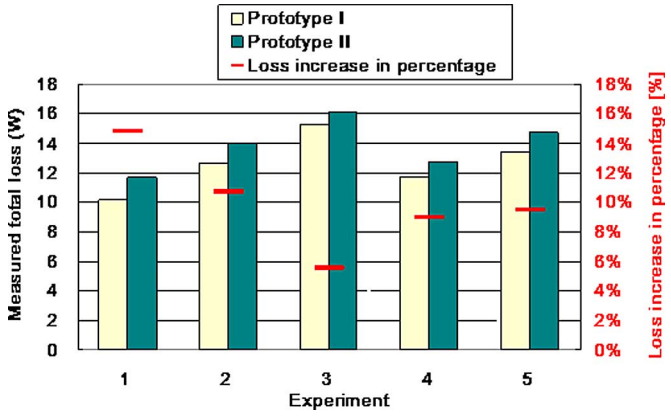

Fig. 15. Total loss measured on prototypes I and II in the two sets experiments, respectively, as well as the loss increase in prototype II with respect to that in prototype I in percentage.

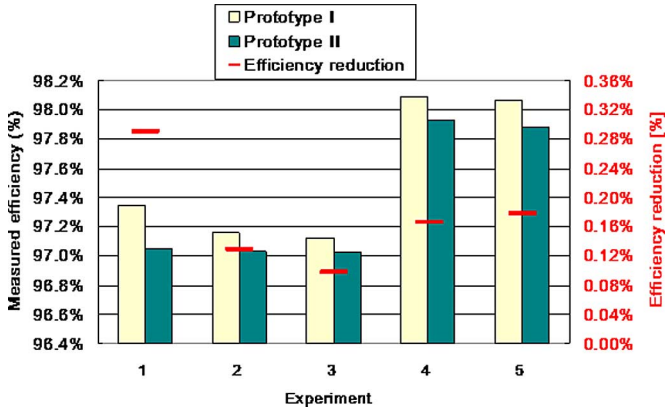

Fig. 16. Efficiency measured on prototypes I and II in the two sets experiments, respectively, and the efficiency reduction in prototype II as compared to that in prototype I.

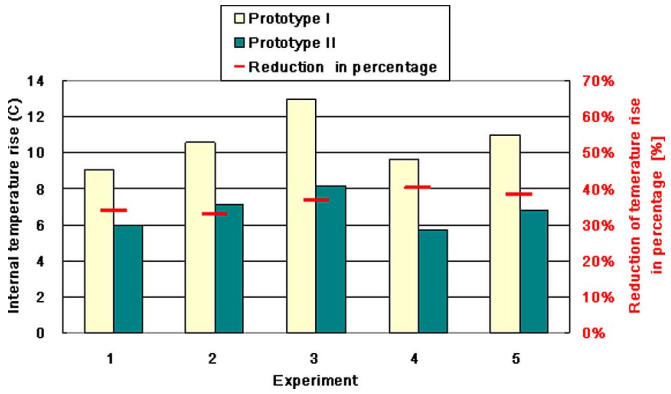

Fig. 17. Internal temperature rise measured on prototypes I and II in the two sets experiments, respectively, and the reduction of temperature rise in percentage with respect to the temperature rise in prototype I.

compared to each other to investigate the performance improvement induced by the heat extractors. By keeping the circuit operation condition and the external cooling condition the same, the two prototypes are tested under a set of the experiments. The power density, efficiency, total loss, and internal temperature rise are recorded for the comparison. The operating points are selected to simplify the verification of loss models. Since the operating frequency impacts not only core loss but also winding loss and dielectric loss, the frequency was kept nearly constant. The varying output voltage and current in different operating points provide different combination of losses in the core, winding, and dielectric layers. The sums of all the losses calculated by the loss models are compared with the measured LLCT total losses (discussed in another paper). Table VI lists the circuit operation conditions of the comparison experiments. The comparison of the total loss of the two prototypes is shown in Fig. 15. Fig. 16 shows the efficiency comparison, and Fig. 17 shows the comparison of the internal temperature rise. The results of the five sets of comparison experiments show that by applying the heat extractors, the total loss of the integrated module increases less than 15%, the efficiency reduces less than 0.32%, while the internal temperature rise reduces more than 30% of that without heat extractors.

The low internal temperature rise indicates that the design was conservative and higher power density can be achieved under the thermal constraints. To further investigate the power density capability of prototype II, four more tests have been done with the throughput power increasing from 450 W to 1 kW. The circuit operation conditions and the test results are listed in Table VII. Prototype II reaches the power density of

TABLE VII
CIRCUIT OPERATION CONDITIONS AND RESULTS OF THE TESTS WITH PROTOTYPE II FOR HIGH POWER DENSITY CAPABILITY INVESTIGATION

Experiment	1	2	3	4
f (kHz)	938	925	954	920
V_{in} (V)	353.4	361.3	367.1	385.5
I_{in} (A)	1.388	2.070	2.633	2.827
$P_{in\_converter}$ (W)	490.5	747.9	966.6	1089.8
V_{out} (V)	47.82	48.44	48.11	51.00
I_{out} (A)	9.51	14.38	18.71	19.77
$P_{out\_converter}$ (W)	454.8	696.6	900.1	1008.3
$P_{loss\_converter}$ (W)	35.7	51.3	66.5	81.5
converter efficiency (%)	92.71%	93.14%	93.13%	92.52%
LLCT loss (W)	13.87	16.57	18.39	21.94
LLCT efficiency (%)	96.95%	97.62%	97.96%	97.82%
LLCT temp. rise (°C)	9.901	11.476	12.425	14.388
LLCT power density (W/in^3) / (W/cm^3)	518 / 32	793 / 48	1024/ 63	1147/ 70

1147 W/in^3 (70 W/cm^3) with the efficiency of 97.8% and the internal temperature rise of 14.39 °C.

VII. Conclusion

This paper presents the investigation of applying heat extractors in integrated power passive modules. The embedded heat extractors influence both the loss distribution and the thermal behavior of the module. Based on the thermal model describing the thermal behavior, four factors affecting the module performance were proposed and studied by numerical methods. Simulation results show that the relative volume of heat extractors has the largest impact on the module performance. The thermal contact resistance on the heat path greatly influences the overall thermal performance. A large thermal contact resistance may limit the performance improvement. The simulation results show that the power density can be improved with the application of heat extractors. Two prototypes are built for the comparison experiments. The experimental results show that the application of heat extractors (occupying 10% of the total volume) greatly reduces more than 30% of the internal temperature rise, while slightly reducing the efficiency, less than 0.32%. The prototype with embedded heat extractors reaches the power density more than 1 kW/in^3 (70 W/cm^3).

With the same mechanism, the application of heat extraction can be extended to other power electronics components such as active integration modules and discrete passive components.

References

[1] J. T. Strydom and J. D. van Wyk, "Electromagnetic design optimization tool for resonant integrated spiral planar power passives (ISP/sup 3/)," *IEEE Trans. Power Electron.*, vol. 20, no. 4, pp. 743–753, Jul. 2005.

[2] J. Dirker, W. Liu, J. D. Van Wyk, and J. P. Meyer, "Embedded solid state heat extraction in integrated power electronic modules," *IEEE Trans. Power Electron.*, vol. 20, no. 3, pp. 694–703, May 2005.

[3] J. D. van Wyk, J. T. Strydom, L. Zhao, and R. Chen, "Review of the development of high density integrated technology for electromagnetic power passives," in *Proc. VDE/IEEE 2nd Int. Conf. Integr. Power Syst.*, Bremen, Germany, Jun. 2002, pp. 25–34.

[4] J. Dirker, W. Liu, J. D. Van Wyk, and J. P. Meyer, "Evaluation of embedded heat extraction for high power density integrated electromagnetic power passives," in *Proc. IEEE Power Electron. Spec. Conf. (PESC'04)*, Aachen, Germany, pp. 4888–4893.

[5] W. Liu and J. D. van Wyk, "Design of integrated LLCT module for LLC resonant converter," in *Proc. IEEE Appl. Power Electron. Conf. Expo. (APEC'05)*, vol. 1, pp. 362–368.

[6] J. Dirker and J. P. Meyer, "Optimum rectangular embedded cooling structure shapes in heat generating mediums—A two-dimensional approach," presented at the 2nd Int. Conf. Heat Transfer, Fluid Mech., Thermodyn. (HEFAT'03), Livingstone, Zambia, paper DJ1.

[7] J. T. Strydom and J. D. van Wyk, "Electromagnetic modeling for design and loss estimation of resonant integrated spiral planar power passives," *IEEE Trans. Power Electron.*, vol. 19, no. 3, pp. 603–617, May 2004.

[8] B. Yang, F. C. Lee, A. J. Zhang, and G. Huang, "LLC resonant converter for front end dc/dc conversion," in *Proc. IEEE Appl. Power Electron. Conf. Expo. (APEC'02)*, vol. 2, pp. 1108–1112.

[9] W. Liu, J. D. van Wyk, and W. G. Odendaal, "Design and evaluation of integrated electromagnetic power passives with vertical surface interconnections," in *Proc. IEEE Appl. Power Electron. Conf. Expo. (APEC'04)*, vol. 2, pp. 22–26.

[10] W. Liu, J. D. van Wyk, and B. Lu, "In-circuit loss measurement of a high-frequency integrated power electronics module," *IEEE Trans. Instrum. Meas.*, vol. 57, no. 7, pp. 1394–1402, Jul. 2008.

Wenduo Liu received the B.Eng. and M.Eng. degrees in mechanical engineering from Tsinghua University, Beijing, China, in 1998 and 2001, respectively, and the Ph.D. degree in electrical engineering from Virginia Polytechnic Institute and State University, Blacksburg, in 2006.

Since 2006, he has been an Electronic Engineer at the International Rectifier Corporation, El Segundo, CA. His current research interests include integration technology and high-frequency high-density power electronics modules.

Jaco Dirker received the B.Eng. (*cum laude*) degree in mechanical engineering in 2000, the B.Sc. (*cum laude*) degree in mathematics and applied mathematics in 2002, the M.Eng. (*cum laude*) degree in mechanical engineering in 2002, and the Ph.D. degree in mechanical engineering in 2004, all from the Rand Afrikaans University, Johannesburg, South Africa.

Since 2004, he has been with the Department of Mechanical and Aeronautical Engineering, University of Pretoria, Pretoria, South Africa, where he was earlier a Lecturer and is currently a Senior Lecturer. His current research interests include conductive and convective heat transfer and cooling of electronics.

Jacobus Daniel van Wyk (M'81–SM'84–F'90) received the M.Sc.Eng. degree from the University of Pretoria, Pretoria, South Africa, in 1966, the Dr.Sc.Tech. degree from the Technical University of Eindhoven, Eindhoven, The Netherlands, in 1969, and the Honorary D.Sc. (Eng.) degree from the University of Natal, KwaZulu-Natal, South Africa, in 1996, as well as the Honorary D.Eng. degree from the University of Pretoria, in 2008, all in electrical engineering.

Between 1961 and 1971, he has worked with the S. A. Iron and Steel Corporation, the University of Pretoria, and as a Member of the Technical and Scientific Staff of the University in Eindhoven. From 1971 to 1995, he was a Chaired Professor of Electrical and Electronic Engineering at the Rand Afrikaans University, Johannesburg, South Africa, holding Chairs in Electronics and in Power Electronics until 1992. He founded the Industrial Electronics Technology Research Group in the Faculty of Engineering in 1978 and directed this until 1999. From 1995 to 2004, he held a special University Research Chair in Industrial Electronics at the Rand Afrikaans University. He joined the Bradley Department of Electrical and Computer Engineering at the Virginia Polytechnic Institute and State University, Blacksburg, VA, in 1999, where he was the J. Byron Maupin Professor of Engineering from 2000 until his retirement in 2005. At Virginia Tech, he was with the National Science Foundation Engineering Research Center for Power Electronics Systems, leading the research on high-density integration until July 2006. During 2006–2008, he was a Research Faculty Member in the Center, and currently, he is a Visiting Professor at the University of Johannesburg. He is the author or coauthor of more than 600 publications, receiving 24 publication awards for this work, including 15 IEEE prize paper awards.

Dr. van Wyk is a Fellow of the South African Institute of Electrical Engineers. He was the recipient of the prestigious IEEE William E. Newell Power Electronics Award in 1995, an IEEE Third Millennium Medal in 2000, the IEEE Power Electronics Society Distinguished Service Award in 2006, and the lifetime IEEE Industry Applications Society Outstanding Achievement Award in 2006. He has received a range of other awards from IEEE Societies, the South African Institute of Electrical Engineers, and other organizations. He was the Editor-in-Chief of the IEEE Transactions on Power Electronics from 2002 to 2006.